Realization of a magneto-optical near-zero index medium by an unpaired Dirac point

Xin Zhou,[1] Daniel Leykam,[2] Udvas Chattopadhyay,[1] A. B. Khanikaev,[3] and Y. D. Chong[1,4,*]

[1]*Division of Physics and Applied Physics, School of Physical and Mathematical Sciences, Nanyang Technological University, Singapore 637371, Singapore*

[2]*Center for Theoretical Physics of Complex Systems, Institute for Basic Science (IBS), Daejeon 34126, Republic of Korea*

[3]*Department of Physics, Queens College and Graduate Center of The City University of New York, Queens, New York 11367, USA*

[4]*Centre for Disruptive Photonic Technologies, Nanyang Technological University, Singapore 637371, Singapore*

(Received 27 December 2017; published 8 November 2018)

We realize an unpaired Dirac cone at the center of the Brillouin zone, using a gyromagnetic photonic crystal with broken square sublattice symmetry and broken time-reversal symmetry. The behavior of the Dirac modes can be described by a gyromagnetic effective medium model with near-zero refractive index, and Voigt parameter near unity. When two domains are subjected to opposite magnetic biases, there exist unidirectional edge states along the domain wall. This establishes a link between topological edge states and the surface waves of homogeneous magneto-optical media.

DOI: 10.1103/PhysRevB.98.205115

I. INTRODUCTION

In two-dimensional (2D) lattices, Dirac points are linear band-crossing points associated with emergent relativistic two-component particles. Since the work of Haldane [1], they have been recognized as the elementary "building blocks" for topological phases, occurring at the boundaries separating parametric domains of different band topology [2,3]. If time-reversal symmetry ($\mathcal{T}$) is unbroken, Dirac points come in pairs [4,5]; in triangular and honeycomb lattices such as graphene, the pairs are pinned to high-symmetry points at the corners of the Brillouin zone [1,6]. By breaking $\mathcal{T}$ and lattice symmetries, however, these constraints can be relaxed.

This paper describes an experimentally realizable $\mathcal{T}$-broken photonic crystal of gyromagnetic cylinders, whose band structure exhibits an unpaired Dirac point at the center of the Brillouin zone (Γ). The unpaired Dirac point causes the photonic crystal to act as an effective electromagnetic medium with two interesting properties: near-zero (NZ) refractive index [7] and strongly enhanced magneto-optical activity. This effective medium description establishes a link between topological edge states and surface waves in magneto-optical NZ media, two phenomena that had previously been conceptually distinct. Unlike the more familiar case of paired Dirac points in triangular or honeycomb photonic crystals, the Dirac modes in our system can be said to act as an effective medium because they interact isotropically with current sources, and there does not exist another valley for them to scatter into.

A number of studies have established the remarkable fact that photonic crystals with conical band-crossing points can act as NZ index effective media [8–12]. Intuitively, this is due to the divergence of the phase velocity near a band-crossing point at Γ. This provides a practical method for using all-dielectric photonic structures to realize NZ index media, which have numerous exotic capabilities such as geometry-insensitive waveguiding [7]. Although the type of band-crossing point utilized in these schemes [8–13] is sometimes called "Dirac-like," due to the conical dispersion, it is not actually described by a Dirac Hamiltonian, as evidenced by the fact that the cone is attached to an inseparable flatband [14,15]. The underlying photonic crystals in these studies are $\mathcal{T}$ symmetric, and so are the effective media, which have NZ refractive index but no magneto-optical activity.

As we have noted, an unpaired Dirac point only exists if $\mathcal{T}$ is broken. If the cone is centered at Γ, it may be described by a NZ index effective medium; but unlike previously studied cases [8–13], the medium exhibits magneto-optical activity (nonvanishing imaginary off-diagonal terms in the permeability tensor). Intriguingly, the enhancement of magneto-optical effects has previously been identified as a promising application of NZ index media. Engheta and co-workers [7,16–18] have noted that the strength of magneto-optical effects is characterized by a Voigt parameter—the ratio of (imaginary) off-diagonal to (real) diagonal components of the permeability or permittivity tensor—which becomes large in NZ index media as the denominator becomes small. We indeed find strong magneto-optical activity in our effective medium, with a near-unity effective Voigt parameter.

Another striking feature of magneto-optical NZ index media is that they can support surface magnetoplasmon-like [19] waves that move unidirectionally along a sample edge without being backscattered by edge deformations and other imperfections [16–18]. The unidirectional and robust nature of these modes is strongly reminiscent of the photonic topological edge states [20] of 2D photonic crystals with topologically nontrivial band structures, whose existence is guaranteed by topological principles. To our knowledge, no definite connection between these two phenomena has previously been identified. The present system sheds light on the issue: the unpaired Dirac point coincides with a topological transition, and as the topological band gap closes, the topological edge states evolve

*yidong@ntu.edu.sg

continuously into the edge states of the magneto-optical NZ index effective medium. In a continuum effective medium theory, such edge states can be characterized by the Chern number as long as the Berry curvature is strongly localized to the Γ point, for example by the material dispersion or by optimization of the full photonic band structure [13,21,22].

The unpaired Dirac point at Γ, like the non-Dirac band-crossing points of Refs. [8–12], is "accidental" in the sense that it must be realized by fine-tuning the lattice; this is consistent with the fact that it appears at a topological transition at finite $\mathcal{T}$ breaking. By contrast, paired Dirac points in $\mathcal{T}$-symmetric lattices, like graphene, can exist without fine-tuning if they are protected by lattice symmetry. (As explained below, however, one of our tuning parameters is the applied magnetic field, which can be tuned continuously in real experiments.) Recently, a photonic system containing an unpaired Dirac point has been proposed [23] and observed [24], based on an array of helical optical waveguides; however, this Dirac point exists in a Floquet band structure defined via the paraxial equations of waveguide mode evolution, which has no straightforward effective medium interpretation. In Ref. [25], it was shown that a $\mathcal{T}$-broken photonic crystal can host an unpaired Dirac point possessing many interesting behaviors, such as one-way Klein tunneling. This Dirac point occurs at a corner of the Brillouin zone (similar to the Haldane model [1]), rather than the Γ point. In principle, such a Dirac point can be moved to Γ by additional fine-tuning.

II. PHOTONIC CRYSTAL STRUCTURE

We will study a photonic crystal based on gyromagnetic rods in a 2D lattice. Similar photonic crystals have previously been used to realize photonic topological insulators [26–31]; in those cases, the $\mathcal{T}$-symmetric band structures contain band-crossing points (either paired Dirac points, or quadratic band-crossing points [32]), and topologically nontrivial gaps are opened as soon as $\mathcal{T}$ is broken by a biasing magnetic field $H \neq 0$ pointing in the out-of-plane ($\hat{z}$) direction. By contrast, we seek a topological transition occurring at a *nonzero* value of H. To achieve this, we search a two-dimensional space spanned by H and a sublattice symmetry-breaking parameter. As shown in Fig. 1(a), we take the unit cell to be a square of lattice constant a, with two ferrite rods lying along the diagonal, surrounded by air. The rods are separated by $a/\sqrt{2}$, and form two square sublattices. They have radii r_1 and r_2, respectively; to further break the sublattice symmetry, we enclose the second rod in a dielectric sheath with refractive index n_2 and outer radius r_s. The ferrite material has dielectric function ϵ_1; when biased by an out-of-plane magnetic field H, its magnetic permeability tensor has the form [33]

$$\overleftrightarrow{\mu} = \begin{bmatrix} \mu & i\alpha & 0 \\ -i\alpha & \mu & 0 \\ 0 & 0 & \mu_0 \end{bmatrix}. \tag{1}$$

The tensor components are given by

$$\mu = 1 + \frac{\omega_m \omega_0}{\omega_0^2 - \omega^2}, \tag{2}$$

$$\alpha = \frac{\omega_m \omega}{\omega_0^2 - \omega^2}, \tag{3}$$

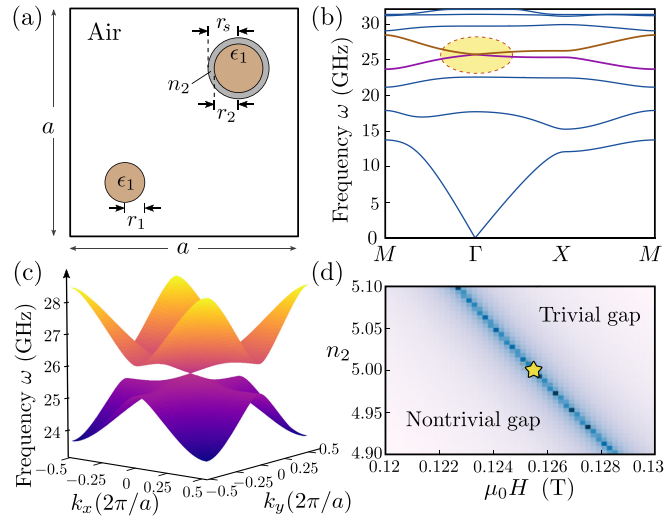

FIG. 1. (a) Schematic of a 2D photonic crystal unit cell: a square of side a, containing two ferrite rods with radii r_1 and r_2, which form square sublattices. One rod has a dielectric cladding with refractive index n_2 and outer radius r_s. We set $a = 4$ cm, $r_1 = 0.088a$, $r_2 = 1.21r_1$, and $r_s = 1.46r_1$. The ferrite has $\epsilon_1 = 15$ and $\mu_0 M_s = 0.191$ T. (b) TM photonic band structure for $n_2 = 5$ and $\mu_0 H = 0.125$ T. Bands 4 and 5 meet at an unpaired Dirac point at Γ. (c) Band structure near the Dirac frequency ($\omega_D = 25.7$ GHz). (d) Heat map (in arbitrary units) showing the minimum frequency separation between bands 4 and 5, versus n_2 and $\mu_0 H$. The Dirac point occurs at a topological band transition; the Chern numbers for the fourth band and fifth band are -1 and 1, respectively, in the nontrivial phase, and both 0 in the trivial phase. The star indicates the parameters used in subplots (b) and (c).

where $\omega_m = g\mu_0 M_s$, $\omega_0 = g\mu_0 H$, $g = 1.76 \times 10^{11}\,\mathrm{C\,kg^{-1}}$ is the gyromagnetic ratio, M_s is the saturation magnetization, and μ_0 is the permeability of free space. Our specific parameter choices are listed in the caption of Fig. 1.

By tuning H and other system parameters, we can generate a Dirac point between bands 4 and 5, as shown in Figs. 1(b)–1(d). The Dirac point appears at Γ (i.e., $k_x = k_y = 0$), with angular frequency $\omega_D \approx 25.7$ GHz, and is unpaired. (These and subsequent numerical results are obtained using COMSOL Multiphysics.) Figure 1(d) plots part of the phase diagram, showing that the Dirac point occurs along a topological phase boundary where $H \neq 0$. The gap is topologically nontrivial; the calculated Chern numbers for the two bands are ± 1 below the critical H, and 0 above. As H decreases further below the depicted range, these two bands undergo another topological transition (featuring a Dirac point at X) and reopen a trivial gap, consistent with the principle that all gaps are topologically trivial for $H = 0$.

The unpaired Dirac point is associated with topological edge states. Figures 2(a)–2(c) show band structures computed for a strip that is periodic along y, and divided along x into two domains with opposite magnetic bias. Below a critical field strength $|H_c|$, there are two branches of gap-spanning edge states on the domain wall, consistent with the Chern number difference of 2 [Fig. 2(a)]. At the transition, the edge states merge continuously into a single branch which passes through the Dirac point [Fig. 2(b)]. Above $|H_c|$, the edge states no

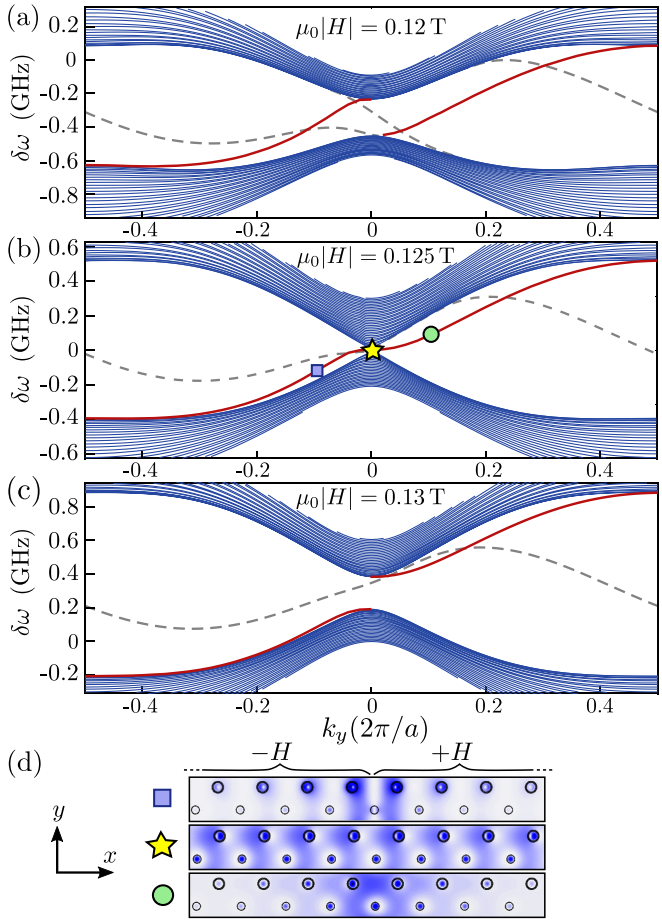

FIG. 2. (a)–(c) Band structures for semi-infinite strip with two domains of opposite magnetic biases $\pm H$. Results are shown for (a) $\mu_0|H| = 0.12$ T (nontrivial gap), (b) $\mu_0|H| = 0.125$ T (unpaired Dirac point), and (c) $\mu_0|H| = 0.13$ T (trivial gap). The angular frequencies are relative to $\omega_D = 25.7$ GHz. The red curves indicate edge states localized at the interface between the domains; gray dashes are spurious edge states localized at the edges of the computational cell. (d) Spatial distributions of field intensity $|E_z|^2$ for the edge states indicated by corresponding symbols in (b). Only the eight unit cells nearest to the domain wall are shown; the actual computational cell is 100 unit cells wide along x.

longer span the band gap [Fig. 2(c)]. At each frequency, the edge states coexist with bulk Dirac modes, but are always centered at the domain wall, as shown in Fig. 2(d). Right at the Dirac point, the edge state delocalizes while the bulk density of states goes to zero.

III. EFFECTIVE MEDIUM DESCRIPTION

We now attempt to describe the Dirac cone using an effective medium with permittivity $\tilde{\epsilon}$, and permeability tensor of the form (1) with parameters $\tilde{\mu}$ and $\tilde{\alpha}$. For TM modes ($E_x = E_y = H_z = 0$), we can show from Maxwell's equations that the bulk dispersion relation is Dirac-like if the medium's frequency dependence satisfies

$$\tilde{\epsilon}\tilde{\mu}\left(1 - \frac{\tilde{\alpha}^2}{\tilde{\mu}^2}\right) = \left[\frac{1}{v_D}\frac{\delta\omega}{\omega}\right]^2, \tag{4}$$

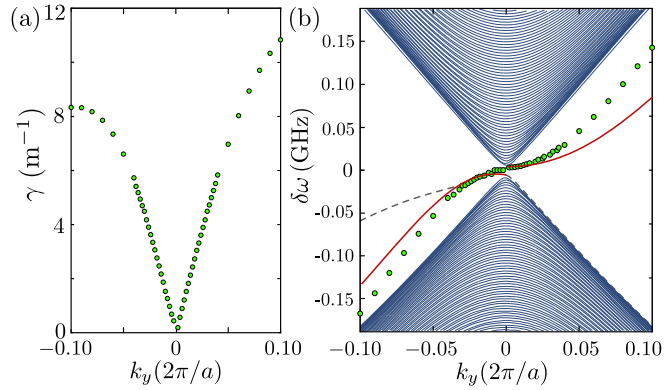

FIG. 3. (a) Edge state decay parameter γ versus k_y. These data are extracted from two-domain photonic crystal simulations by fitting $\langle|E_z|^2\rangle$ (averaged over each unit cell) to an $\exp(-2\gamma|x|)$ envelope. (b) Close-up of the band structure near the Dirac point. The solid curves show the numerically calculated dispersion for the edge states (red) and bulk states (blue); the dashes are spurious edge states localized at edges of the computational cell, which is 300 unit cells wide with all other parameters the same as in Fig. 2(b). The green dots show the effective medium prediction, calculated using the fitted value of v_D and the decay parameters from (a).

where v_D is the Dirac speed, $\delta\omega \equiv \omega - \omega_D$, and ω_D is the Dirac frequency (see Appendix A).

Now consider two uniform domains with equal and opposite Voigt parameters $\tilde{\alpha}/\tilde{\mu}$, separated by a straight domain wall parallel to y. Maxwell's equations support TM modes confined to the domain wall by the mismatch in $\tilde{\alpha}/\tilde{\mu}$. If Eq. (4) is obeyed, these satisfy

$$|\delta\omega| = v_D\sqrt{1 - (\tilde{\alpha}/\tilde{\mu})^2}\,|k_y|, \tag{5}$$

$$\gamma = (\tilde{\alpha}/\tilde{\mu})\,k_y, \tag{6}$$

where k_y is the wave number along the domain wall and $1/\gamma$ is the penetration depth. In order for the modes to decay away from the domain wall, we require $\gamma > 0$.

It should be noted that similar edge states can exist if $\tilde{\epsilon}$, $\tilde{\mu}$, and $\tilde{\alpha}$ are frequency independent [so that Eq. (4) does *not* hold]. In that case, the edge dispersion relation (5) is replaced by

$$\omega = v_0\sqrt{1 - (\tilde{\alpha}/\tilde{\mu})^2}\,|k_y|, \tag{7}$$

where v_0 is the speed of light in the bulk. Then $k_y \to 0$ at zero frequency, rather than a finite Dirac frequency ω_D.

Equations (4)–(6) can be systematically fitted to photonic crystal simulations. From the bulk band diagram, we estimate $v_D \approx 1.26 \times 10^7$ ms^{-1}; the Dirac cone is nearly isotropic, with fits along different crystal axes giving less than 0.5 % variation in v_D. Next, we extract γ by calculating the intensity profile $\langle|E_z|^2\rangle$ for the photonic crystal edge states, averaging over each unit cell, and fitting to an envelope $I_0\exp(-2\gamma|x|)$. The results are shown in Fig. 3(a). Comparing this to Eq. (6), we deduce that the Voigt parameter $\tilde{\alpha}/\tilde{\mu}$ switches sign across ω_D; very near ω_D, it has almost constant magnitude $|\tilde{\alpha}/\tilde{\mu}| \approx 0.94$. From Eq. (4), this also implies that $\tilde{\epsilon}\tilde{\mu} \to 0$ as $\omega \to \omega_D$. Finally, we use the fitted values of v_D and γ together

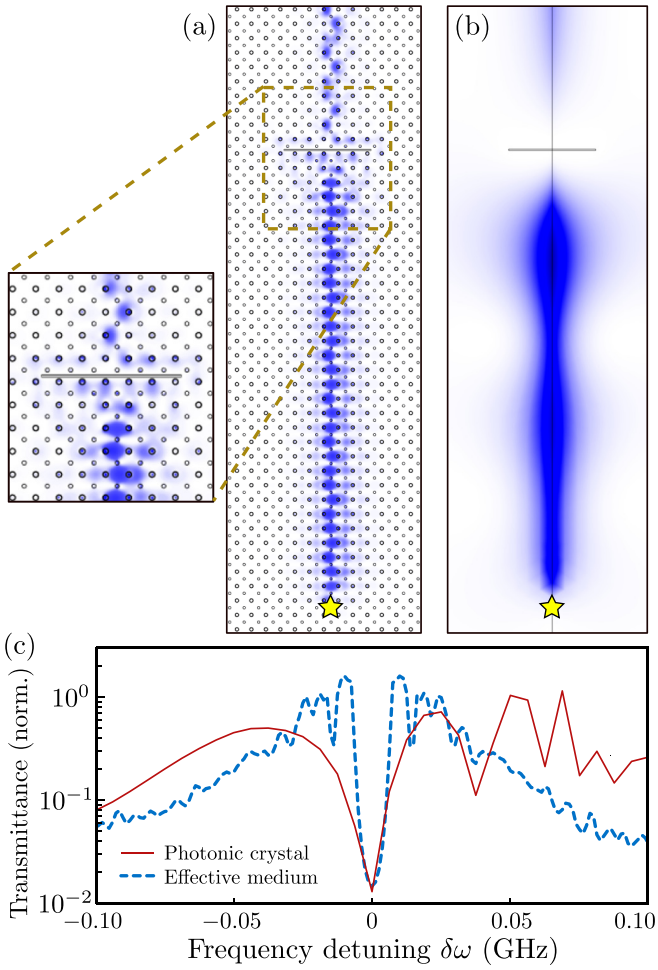

FIG. 4. (a),(b) Spatial distribution of the field intensity $|E_z|^2$, for surface waves moving along a domain wall with a perfect electrical conductor obstacle. (a) Photonic crystal simulation, including an expanded view of the region near the obstacle. (b) Effective medium simulation, using the effective medium fitting parameters from Fig. 3(b). The source positions are indicated by yellow stars. In both cases, the detuning is $\delta\omega \approx 0.04$ GHz. For the effective medium, however, the Dirac frequency is taken to be $\omega_D \approx 25.23$ GHz, a reduction of 1.8% relative to the bulk band-structure calculation; this value is determined from the transmittance dip in (c), and appears to be a discretization error. (c) Transmittance versus frequency detuning $\delta\omega$, for the photonic crystal and the effective medium model. The transmittance is estimated as the ratio of intensity $25a$ past the obstacle to the intensity $15a$ before the obstacle, along the domain wall.

with Eqs. (5) and (6) to plot the edge state dispersion curve $\delta\omega = \pm v_D\sqrt{k_y^2 - \gamma^2}$. As shown in Fig. 5(b), near the Dirac frequency the dispersion curve predicted by the effective medium theory agrees with the edge state dispersion curve from the photonic crystal simulations.

The effective Voigt parameter of $|\tilde{\alpha}/\tilde{\mu}| \approx 0.94$ is close to the maximum allowed value; it cannot exceed unity, as such a medium would lie in the "Hall opacity" regime [16] where no propagating bulk modes exist. The actual Voigt parameter within the underlying ferrite rods is $\alpha/\mu \approx 1.53$ at the operating frequency. However, the rods occupy only 6% of the photonic crystal's area, so an area-weighted homogenization of the photonic crystal yields an effective Voigt parameter of only $\approx$0.09, while a different homogenization scheme for magneto-optical media [34] yields $\approx$0.24 (see Appendix B). Thus, the Voigt parameter of the Dirac point-induced effective medium is substantially enhanced relative to the homogenized photonic crystal, in agreement with previous arguments that NZ index media can enhance magneto-optical activity [7,16–18].

Although the edge states delocalize ($\gamma \to 0$) at the Dirac frequency, transmission along the edge appears to be quite robust *near* the Dirac frequency. This is due to (i) the reduction in the density of bulk states available to scatter into, and (ii) the fact that the edge states are unidirectional and thus unable to backscatter. Figure 4 shows the transmission along a domain wall with a perfect electrical conductor obstacle. The simulations for both the photonic crystal and the effective medium show a transmittance dip at the Dirac frequency, as shown in Fig. 4(c). At small detunings, the surface waves are able to partially bypass the obstacle, as shown by the field intensity plots in Fig. 4(a) for the photonic crystal, and Fig. 4(b) for the effective medium.

IV. CONCLUSION

We have designed a realistic gyromagnetic photonic crystal with an unpaired Dirac point at Γ. The Dirac medium serves as a magneto-optical NZ index effective medium [7–12,16–18], and we have identified the "remnant" of the topological edge state with the magnetoplasmon-like surface states of the effective medium. The effective Voigt parameter is $\approx$0.94, which is very near the "Hall opacity" regime [16], and enhanced by approximately fourfold relative to the homogenized value. We have focused on the behavior of domain walls in the bulk of an otherwise homogeneous photonic crystal. For finite arbitrarily shaped domains, however, the effective medium description of a photonic crystal is known to be quite approximate, as it assumes the Bloch modes of interest have a dominant Fourier component, which is typically not the case for higher bands [35]. Moreover, if domain boundaries do not preserve the bulk symmetries of the underlying crystal, the effective medium must be complemented by additional mode-matching boundary layers [36]. In the future, it would be interesting to identify models exhibiting unpaired Dirac cones in lower bands, which might mitigate these limitations [8].

ACKNOWLEDGMENTS

We are grateful to C. T. Chan for his stimulating and insightful comments. This work was supported by the Singapore MOE Academic Research Fund Tier 2 Grant No. MOE2015-T2-2-008, the Singapore MOE Academic Research Fund Tier 3 Grant No. MOE2016-T3-1-006, and the Institute for Basic Science in Korea (IBS-R024-Y1).

APPENDIX A: EFFECTIVE MEDIUM THEORY

We seek an effective medium which can be mapped to the gyromagnetic photonic crystal. Maxwell's equations in a

gyromagnetic medium, with no free charges or currents, are

$$\nabla \times \mathbf{E} = i\omega \overleftrightarrow{\mu} \mathbf{H}, \tag{A1}$$

$$\nabla \times \mathbf{H} = -i\omega\epsilon \mathbf{E}, \tag{A2}$$

$$\nabla \cdot (\epsilon \mathbf{E}) = 0, \tag{A3}$$

$$\nabla \cdot (\mu \mathbf{H}) = 0. \tag{A4}$$

Here, ϵ is the scalar permittivity, and the permeability has the form

$$\overleftrightarrow{\mu} = \begin{bmatrix} \mu & i\alpha & 0 \\ -i\alpha & \mu & 0 \\ 0 & 0 & \mu_0 \end{bmatrix}. \tag{A5}$$

Assume a uniform medium, so that both ϵ and $\overleftrightarrow{\mu}$ are position independent. We consider TM modes with $E_x = E_y = H_z = 0$. For this polarization, Eq. (A3) is automatically satisfied. Combining Eq. (A1) with Eq. (A5) gives

$$-\nabla_{2\mathrm{D}}^2 E_z = i\omega[\mu(\partial_x H_y - \partial_y H_x) - i\alpha(\partial_x H_x + \partial_y H_y)], \tag{A6}$$

where $\nabla_{2\mathrm{D}}^2 \equiv \partial_x^2 + \partial_y^2$ is the 2D Laplacian. Next, combining Eq. (A4) with Eq. (A5) gives

$$\mu(\partial_x H_x + \partial_y H_y) = -i\alpha(\partial_x H_y - \partial_y H_x). \tag{A7}$$

Combining Eqs. (A6) and (A7) and Eq. (A2) yields

$$\left[\nabla_{2\mathrm{D}}^2 + \epsilon\mu\left(1 - \frac{\alpha^2}{\mu^2}\right)\omega^2\right] E_z = 0. \tag{A8}$$

So far, we have not made any assumptions about the frequency dispersion of the medium. We now assume that the bulk dispersion obeys the Dirac dispersion relation

$$\omega = \omega_D + v_D|\mathbf{k}|, \tag{A9}$$

where ω_D is the Dirac frequency, v_D is the effective speed of the Dirac modes, and $\mathbf{k} = (k_x, k_y)$ is the 2D in-plane wave vector. Comparing Eqs. (A8) and (A9), we deduce that

$$\epsilon\mu\left(1 - \frac{\alpha^2}{\mu^2}\right) = \left[\frac{1}{v_D}\frac{\delta\omega}{\omega_D}\right]^2, \tag{A10}$$

where $\delta\omega \equiv \omega - \omega_D$ (we assume throughout that $|\delta\omega| \ll \omega_D$). This means that the effective refractive index vanishes for $\delta\omega \to 0$; this is a NZ index medium.

Next, consider two adjacent domains, separated by a domain wall at $x = 0$. The magnetic bias has opposite signs for $x > 0$ and $x < 0$. In other words, for $x < 0$ we replace α with $-\alpha$ in Eq. (A5). We now seek solutions of the form

$$E_z = E_0\, e^{-\gamma|x| + ik_y y}. \tag{A11}$$

These modes are localized around $x = 0$, with wave number k_y parallel to the domain wall and penetration depth $1/\gamma$. Note that E_z is necessarily continuous across the domain wall. Substituting into Eq. (A8) yields the condition

$$k_y^2 - \gamma^2 = \epsilon\mu\left(1 - \frac{\alpha^2}{\mu^2}\right)\omega^2. \tag{A12}$$

Moreover, knowing E_z we can use Eq. (A1) to retrieve the magnetic fields:

$$\mathbf{H} = \frac{1}{i\omega}\overleftrightarrow{\mu}^{-1} \nabla \times \mathbf{E}, \tag{A13}$$

$$\begin{bmatrix} H_x \\ H_y \end{bmatrix} = \frac{E_0}{i\omega}\overleftrightarrow{\mu}^{-1}\begin{bmatrix} ik_y \\ \pm\gamma \end{bmatrix} e^{\mp\gamma x + ik_y y} \tag{A14}$$

$$= \frac{E_0}{i\omega(\mu^2 - \alpha^2)}\begin{bmatrix} i(\mu k_y - \alpha\gamma) \\ \pm(\mu\gamma - \alpha k_y) \end{bmatrix} e^{\mp\gamma x + ik_y y}, \tag{A15}$$

where the $\pm$ signs denote the $x > 0$ and $x < 0$ domains, respectively. Due to the absence of surface currents, H_y must also be continuous across the domain wall, and hence

$$\gamma = \frac{\alpha k_y}{\mu}. \tag{A16}$$

The parameter γ must be positive. Eq. (A16) implies that if a domain wall state exists for $k_y > 0$, then $\alpha/\mu > 0$ for $k_y > 0$. Conversely, if a domain wall state exists for $k_y < 0$, then $\alpha/\mu < 0$ for $k_y < 0$. In Figs. 2(b) and 3, we observe that domain wall states of the photonic crystal exist for both positive and negative k_y. Moreover, the domain wall state's relative frequency $\delta\omega \equiv \omega - \omega_D$ switches sign as k_y switches sign. This implies that α/μ switches sign across the Dirac frequency.

Using Eq. (A16), we can simplify Eq. (A12) to $\epsilon\mu\omega^2 = k_y^2$. Applying the Dirac medium condition (A10) then yields the dispersion relation for the domain wall states:

$$\delta\omega^2 = v_D^2\left[1 - \left(\frac{\alpha}{\mu}\right)^2\right]k_y^2. \tag{A17}$$

We now estimate v_D by taking the dispersion along two directions, Γ-X and Γ-M. The values of v_D and ω_D estimated for both cases are almost identical, and we take the mean values $v_D = 1.998 \times 10^6$ ms^{-1} and $\omega_D = 4.09$ GHz. By fitting the penetration constant of the domain wall states to Eq. (A16), we find $|\alpha/\mu| \approx 0.94$, independent of the sign of k_y [see Fig. 3(a)]. This implies, via Eq. (A17), that the domain wall states have a linear dispersion relation, with group velocity

$$v_s = v_D\sqrt{1 - \frac{\alpha^2}{\mu^2}}. \tag{A18}$$

Since $|\alpha/\mu|$ is close to unity, $v_s \ll v_D$.

APPENDIX B: EFFECTIVE VOIGT PARAMETER UNDER CRUDE HOMOGENIZATION

In Sec. III, we pointed out that the effective medium has an effective Voigt parameter of $|\tilde{\alpha}/\tilde{\mu}| \approx 0.94$. Given that the rods occupy only 6% of the photonic crystal's area, an area-weighted estimation of the Voigt parameter would predict only $\alpha/\mu \approx 0.092$, which is an order of magnitude lower.

To better quantify the enhancement in the effective Voigt parameter, we can perform a homogenization based on medium parameters and filling fractions. A scheme for homogenizing magneto-optic media was derived in Ref. [34]. That paper considered cylinders of gyroelectric material, with

dielectric tensors of the form

$$\overleftrightarrow{\epsilon}_2 = \begin{bmatrix} \epsilon_2 & i\gamma & 0 \\ -i\gamma & \epsilon_2 & 0 \\ 0 & 0 & \epsilon_2 \end{bmatrix}. \tag{B1}$$

The background medium has permittivity ϵ_1, and the magnetic permeability is unity throughout. It was found that the homogenized effective dielectric parameters are

$$\tilde{\epsilon}_{x,y} = \epsilon_1 + f(\epsilon_2 - \epsilon_1)\left[1 + \frac{(1-f)(\epsilon_2-\epsilon_1)}{2\epsilon_1}\right]^{-1}, \tag{B2}$$

$$\tilde{\epsilon}_z = (1-f)\epsilon_1 + f\epsilon_2, \tag{B3}$$

$$\tilde{\gamma} = \gamma f\left[1 + \frac{(1-f)(\epsilon_2-\epsilon_1)}{2\epsilon_1}\right]^{-1}, \tag{B4}$$

where $\tilde{\epsilon}_x$, $\tilde{\epsilon}_y$, and $\tilde{\epsilon}_z$ are the on-diagonal components, and $\tilde{\gamma}$ is the magneto-optical off-diagonal component of the effective permittivity tensor, and f is the volume fraction of the gyroelectric component.

We adapt this calculation to our gyromagnetic photonic crystal by the mapping

$$\begin{Bmatrix} \nabla \times \mathbf{E} = i\omega\mathbf{B} \\ \nabla \times \mathbf{B} = -i\omega\overleftrightarrow{\epsilon}\mathbf{E} \\ \mu = 1 \end{Bmatrix} \leftrightarrow \begin{Bmatrix} \nabla \times \mathbf{B} = -i\omega\mathbf{E} \\ \nabla \times \mathbf{E} = i\omega\overleftrightarrow{\mu}\mathbf{H} \\ \epsilon = 1 \end{Bmatrix}. \tag{B5}$$

As this is only intended as a crude comparison, we ignore the nonunity permittivities of the ferrite rods. At the operating frequency of $\omega \approx 25.7$ GHz, the ferrite permeability parameters are $\mu \approx -3.19$ and $\alpha \approx -4.90$. The volume fraction is $f \approx 0.06$. Thus,

$$\tilde{\mu} = 1.26, \quad \tilde{\alpha} = 0.30. \tag{B6}$$

This corresponds to a Voigt parameter of $\tilde{\alpha}/\tilde{\mu} \approx 0.24$.

[1] F. D. M. Haldane, Model for a Quantum Hall Effect without Landau Levels: Condensed-Matter Realization of the Parity Anomaly, Phys. Rev. Lett. **61**, 2015 (1988).

[2] M. Z. Hasan and C. L. Kane, "Colloquium: Topological insulators," Rev. Mod. Phys. **82**, 3045 (2010).

[3] X.-L. Qi and S.-C. Zhang, "Topological insulators and superconductors," Rev. Mod. Phys. **83**, 1057 (2011).

[4] H. B. Nielsen and M. Ninomiya, Absence of neutrinos on a lattice: (I) proof by homotopy theory, Nucl. Phys. B **185**, 20 (1981).

[5] H. B. Nielsen and M. Ninomiya, Absence of neutrinos on a lattice: (II) intuitive topological proof, Nucl. Phys. B **193**, 173 (1981).

[6] G. W. Semenoff, Condensed-Matter Simulation of a Three-Dimensional Anomaly, Phys. Rev. Lett. **53**, 2449 (1984).

[7] I. Liberal and N. Engheta, Near-zero refractive index photonics, Nat. Photonics **11**, 149 (2017).

[8] X. Huang, Y. Lai, Z. H. Hang, H. Zhen, and C. T. Chan, Dirac cones induced by accidental degeneracy in photonic crystals and zero-refractive-index materials, Nat. Mater. **10**, 582 (2011).

[9] C. T. Chan, Z. H. Hang, and X. Huang, Dirac dispersion in two-dimensional photonic crystals, Adv. Opt. Electron. **2012**, 313984 (2012).

[10] J. W. Dong, M. L. Chang, X. Q. Huang, Z. H. Hang, Z. C. Zhong, W. J. Chen, Z. Y. Huang, and C. T. Chan, Conical Dispersion and Effective Zero Refractive Index in Photonic Quasicrystals, Phys. Rev. Lett. **114**, 163901 (2015).

[11] M. W. Ashraf and M. Faryad, On the mapping of Dirac-like cone dispersion in dielectric photonic crystals to an effective zero-index medium, J. Opt. Soc. Am. B **33**, 1008 (2016).

[12] S. Jahani and Z. Jacob, All-dielectric metamaterials, Nat. Nanotechnol. **11**, 23 (2016).

[13] M. Xiao and S. Fan, Photonic Chern insulator through homogenization of an array of particles, Phys. Rev. B **96**, 100202(R) (2017).

[14] D. Green, L. Santos, and C. Chamon, Isolated flat bands and spin-1 conical bands in two-dimensional lattices, Phys. Rev. B **82**, 075104 (2010).

[15] D. Leykam and A. S. Desyatnikov, Conical intersections for light and matter waves, Adv. Phys. X **1**, 101 (2016).

[16] A. R. Davoyan and N. Engheta, Theory of Wave Propagation in Magnetized Near-Zero-Epsilon Metamaterials: Evidence for One-Way Photonic States and Magnetically Switched Transparency and Opacity, Phys. Rev. Lett. **111**, 257401 (2013).

[17] A. R. Davoyan, A. M. Mahmoud, and N. Engheta, Optical isolation with epsilon-near-zero metamaterials, Opt. Express **21**, 3279 (2013).

[18] F. Abbasi, A. R. Davoyan, and N. Engheta, One-way surface states due to nonreciprocal lightline crossing, New J. Phys. **17**, 063014 (2015).

[19] B. Hu, Y. Zhang, and Q. J. Wang, Surface magneto plasmons and their applications in the infrared frequencies, Nanophotonics **4**, 383 (2015).

[20] L. Lu, J. D. Joannopoulos, and M. Soljačić, Topological photonics, Nat. Photonics **8**, 821 (2014).

[21] M. G. Silveirinha, Chern invariants for continuous media, Phys. Rev. B **92**, 125153 (2015).

[22] M. G. Silveirinha, Bulk-edge correspondence for topological photonic continua, Phys. Rev. B **94**, 205105 (2016).

[23] D. Leykam, M. C. Rechtsman, and Y. D. Chong, Anomalous Topological Phases and Unpaired Dirac Cones in Photonic Floquet Topological Insulators, Phys. Rev. Lett. **117**, 013902 (2016).

[24] J. Noh, S. Huang, D. Leykam, Y. D. Chong, K. P. Chen, and M. C. Rechtsman, Experimental observation of optical Weyl points and Fermi arc-like surface states, Nat. Phys. **13**, 611 (2017).

[25] X. Ni, D. Purtseladze, D. A. Smirnova, A. Slobozhanyuk, A. Alù, and A. B. Khanikaev, Spin and valley polarized one-way Klein tunneling in photonic topological insulators, Sci. Adv. **4**, eaap8802 (2018).

[26] F. D. M. Haldane and S. Raghu, Possible Realization of Directional Optical Waveguides in Photonic Crystals with Broken Time-Reversal Symmetry, Phys. Rev. Lett. **100**, 013904 (2008).

[27] S. Raghu and F. D. M. Haldane, Analogs of quantum-Hall-effect edge states in photonic crystals, Phys. Rev. A **78**, 033834 (2008).

[28] Z. Wang, Y. D. Chong, J. D. Joannopoulos, and M. Soljačić, Reflection-Free One-Way Edge Modes in a Gyromagnetic Photonic Crystal, Phys. Rev. Lett. **100**, 013905 (2008).

[29] Z. Wang, Y. Chong, J. D. Joannopoulos, and M. Soljačić, Observation of unidirectional backscattering-immune topological electromagnetic states, Nature (London) **461**, 772 (2009).

[30] J.-X. Fu, R.-J. Liu, and Z.-Y. Lia, Robust one-way modes in gyromagnetic photonic crystal waveguides with different interfaces, Appl. Phys. Lett. **97**, 041112 (2010).

[31] Y. Poo, R. Wu, Z. Lin, Y. Yang, and C. T. Chan, Experimental Realization of Self-Guiding Unidirectional Electromagnetic Edge States, Phys. Rev. Lett. **106**, 093903 (2011).

[32] Y. D. Chong, X.-G. Wen, and M. Soljačić, Effective theory of quadratic degeneracies, Phys. Rev. B **77**, 235125 (2008).

[33] D. M. Pozar, *Microwave engineering* (Wiley, New York, 1998).

[34] M. Abe and M. Gomi, Magneto-optical effect and effective dielectric tensor in composite material containingmagnetic fine particles or thin layers, Jpn. J. Appl. Phys. **23**, 1580 (1984).

[35] W. Smigaj and B. Gralak, Validity of effective-medium approximation of photonic crystals, Phys. Rev. B **77**, 235445 (2008).

[36] C. R. Simovski, On electromagnetic characterization and homogenization of nanostructured metamaterials, J. Opt. **13**, 013001 (2011).